International Journal of Thermophysics, Vol. 25, No. 5, September 2004 (© 2004)

Analysis of Photothermal Characterization of Layered Materials – Design of Optimal Experiments[1]

K. D. Cole[2]

In this paper numerical calculations are presented for the steady-periodic temperature in layered materials and functionally-graded materials to simulate photothermal methods for the measurement of thermal properties. No laboratory experiments were performed. The temperature is found from a new Green's function formulation which is particularly well-suited to machine calculation. The simulation method is verified by comparison with literature data for a layered material. The method is applied to a class of two-component functionally-graded materials, and results for temperature and sensitivity coefficients are presented. An optimality criterion, based on the sensitivity coefficients, is used for choosing what experimental conditions will be needed for photothermal measurements to determine the spatial distribution of thermal properties. This method for optimal experiment design is completely general and may be applied to any photothermal technique and to any material with spatial variation of thermal properties.

KEY WORDS: functionally graded material; Green's functions; optimal experiment; photothermal; thermal properties.

1. INTRODUCTION

Functionally graded (FG) materials are being studied as possible components of aero-space thermal protection systems. These materials include composites with epoxy and metal matrices, metal foams, or any structure with properties designed to vary with position. In the future when FG materials are specified as part of a vehicle program, part of the

[1] Paper presented at the Fifteenth Symposium on Thermophysical Properties, June 22–27, 2003, Boulder, Colorado, U.S.A.

[2] Mechanical Engineering Department, University of Nebraska–Lincoln, Lincoln, Nebraska 68588-0656, U.S.A. E-mail: kcole1@unl.edu

0195-928X/04/0900-1567/0 © 2004 Plenum Publishing Corporation

procurement process will involve certification that the material meets the specifications.

To date there has been little research on accurate thermal characterization of FG materials. The present research is intended to close this gap in the procurement cycle by investigating photothermal methods for non-destructive and accurate measurement of thermal properties in FG materials. In this paper only numerical simulations are presented and no laboratory experiments were performed.

A review of the pertinent literature is given next in three areas: computer simulation of FG materials; heat transfer theory for photothermal methods; and, optimal experiment design.

Several researchers have found analytical solutions for the thermal response by representing a FG material as composed of multiple layers each with different, spatially uniform, thermal properties [1–3]. One study investigated an exponential-function variation of thermal properties along one spatial direction [4]. Another used Galerkin's method to find the temperature in materials with arbitrary property distributions [5]. The primary motivation for these studies has been to determine the temperature for the purpose of finding thermal stresses, or to find the distribution of thermal properties that optimizes the thermal stresses [6, 7].

One research group has reported transient-heating experiments to measure thermal properties in a FG material [8,9]. This group studied a FG material containing an exponentially varying spatial distribution of thermal properties. Their data analysis combines a single temperature datum with their transient theory to provide a single value for the parameter describing the spatial distribution of thermal properties. Although simple in concept, this approach is sensitive to measurement noise.

In the area of photothermal measurements, there are several pertinent publications. A diverse collection of thermal-wave Green's functions and temperature solutions has been published recently in book form [10]. Primarily homogeneous materials are treated, and layered materials are included by defining a global Green's function that embodies the effects of several layers in the material. Because the complexity of the layered-body Green's function increases rapidly as layers are added, no more than three layers are discussed.

Theory for the thermal response of a many-layered body has been studied previously by the author [11, 12]. The laser heating is treated exactly from the optical absorption properties of all layers. The multi-layer body is efficiently described by local Green's functions which are found first in the time domain and are then transformed into the frequency domain. Each layer is linked to adjacent layers with appropriate interface conditions.

Theory for the photoacoustic response of a layered solid has been recently reported in which the temperature in each layer is linked with

adjacent layers by interface conditions [13]. The optical absorption in each solid layer is described by an exponential distribution and an absorption coefficient. The photoacoustic response is found from both thermal effects and mechanical effects in the gas; however, thermal effects predominate for solid materials. The method is used for analysis of experimental data in materials with two and three layers.

In the area of optimal experiment design, parameter estimation has been used for obtaining thermal properties from transient experiments for many years [14]. In these methods the desired parameters are found by non-linear regression between the experimental data (temperatures in this case) and a computational model of the experiment. Parameter estimation concepts have recently been applied to optimal experiment design for thermal characterization of uniform materials [15] and for materials with temperature-varying properties [16]. The author has previously studied optimal experiment design for low-conductivity FG materials [17]. The simulated experiments involved time-series data collected from one or more temperature sensors, and the data analysis is carried out in the time domain. An optimality criterion was used to find the best experimental conditions for simultaneous estimation of several thermal properties. Results of simulations show that for FG materials with spatially varying conductivity, it is better to heat the sample from the low-conductivity side.

In the present paper, FG materials are simulated with a large number of interconnected layers. The heat transfer theory draws upon the author's previous work with Green's functions, but here the Green's functions are given directly in the frequency domain in the form of algebraic expressions, not infinite-series expressions, that are numerically well behaved under all conditions. Likewise, the temperature expressions found from these Green's functions are numerically well behaved. The Green's functions are given for a variety of boundary conditions; previously only specified-flux boundaries were treated. To the author's knowledge this paper describes the first application of optimal experiment design methods to frequency-domain analysis appropriate for photothermal experiments. This paper is divided into several sections, as follows: the temperature in one layer; the Green's functions; the temperature in a multi-layer material; the design of optimal experiments; results for a layered material; results for a FG material; and, a brief summary.

2. TEMPERATURE IN ONE LAYER

Consider first a single layer in which the temperature is sought. The temperature distribution satisfies

$$\frac{\partial^2 \tilde{T}}{\partial x^2} - \frac{1}{\alpha}\frac{\partial \tilde{T}}{\partial t} = \frac{1}{k}\tilde{g}(x,t),$$
$$k_i \frac{\partial \tilde{T}}{\partial n_i} + h_i \tilde{T} = \tilde{f}_i(t) \quad \text{at boundary } i = 1, 2. \tag{1}$$

Here α is the thermal diffusivity ($m^2 \cdot s^{-1}$), k is the thermal conductivity ($W \cdot m^{-1} \cdot K^{-1}$), $\tilde{g}$ is the volume heating ($W \cdot m^{-3}$) deposited by a laser, and $\tilde{f}_i$ is a specified boundary condition. Index $i = 1, 2$ represents the boundaries at the limiting values of coordinate x. The boundary condition may be one of three types at each boundary: boundary type 1 is specified temperature ($k_i = 0$ and $h_i = 1$); boundary type 2 is specified heat flux ($h_i = 0$); and, boundary type 3 is specified convection where h_i is a constant-with-time heat transfer coefficient (or contact conductance).

Since the photothermal applications of interest involve periodic heating by a laser, the solution is sought in Fourier-transform space, and the solution is interpreted as the steady-periodic response at a single frequency ω. For further discussion of this point see Ref. 18. Consider the Fourier transform of the above temperature equations:

$$\frac{\partial^2 T}{\partial x^2} - \frac{j\omega}{\alpha} T = -\frac{1}{k} g(x, \omega),$$
$$k_i \frac{\partial T}{\partial n_i} + h_i T = f_i(\omega) \quad \text{at boundaries } i = 1, 2. \tag{2}$$

Here T is the Fourier-space temperature ($K \cdot s$), g is the Fourier-space volume heating ($W \cdot s \cdot m^{-3}$) deposited by a laser, and f_i is the Fourier-space specified boundary condition.

The temperature will be found with the Fourier-space Green's function, defined by the following equations:

$$\frac{\partial^2 G}{\partial x^2} - \sigma^2 G = -\frac{1}{\alpha}\delta(x - x'), \tag{3}$$
$$k_i \frac{\partial G}{\partial n_i} + h_i G = 0, \quad i = 1, 2. \tag{4}$$

Here $\sigma^2 = j\omega/\alpha$ and $\delta(x - x')$ is the Dirac delta function. The coefficient $1/\alpha$ preceding the delta function in Eq. (3) provides the frequency-domain Green's function with units of $s \cdot m^{-1}$. This is consistent with our earlier work with time-domain Green's functions.

Assume for the moment that the Green's function G is known, then the steady-periodic temperature is given by the following integral equation (see Ref. 19, pp. 40–43):

$$T(x,\omega)=\frac{\alpha}{k}\int g(x',\omega)G(x,x',\omega)dx' \quad \text{(for volume heating)}$$
$$+\alpha f_i(\omega)\times\begin{bmatrix}\partial G/\partial n'(x,x_i,\omega) & \text{(type 1 only)}\\ \frac{1}{k}G(x,x_i,\omega) & \text{(type 2 or 3)}\end{bmatrix}, \quad i=1,2. \quad (5)$$

3. GREEN'S FUNCTION

The Green's function (GF) that satisfies Eqs. (3) and (4) is given by

$$G(x,x',\omega)=\frac{S_2^-(S_1^-e^{-\sigma(2L-|x-x'|)}+S_1^+e^{-\sigma(2L-x-x')})}{2\alpha\sigma(S_1^+S_2^+-S_1^-S_2^-e^{-2\sigma L})}$$
$$+\frac{S_2^+(S_1^+e^{-\sigma(|x-x'|)}+S_1^-e^{-\sigma(x+x')})}{2\alpha\sigma(S_1^+S_2^+-S_1^-S_2^-e^{-2\sigma L})}, \quad (6)$$

where the subscripts 1 and 2 represent the two boundaries at the smallest and largest x-values, respectively. Coefficients S_M^+ and S_M^- depend on the boundary conditions on side M and are given by

$$S_M^+=\begin{cases}1 & \text{if side } M \text{ is type 0, type 1, or type 2,}\\ k\sigma+h_M & \text{if side } M \text{ is type 3,}\end{cases}$$

$$S_M^-=\begin{cases}0 & \text{if side } M \text{ is type 0,}\\ -1 & \text{if side } M \text{ is type 1,}\\ 1 & \text{if side } M \text{ is type 2,}\\ k\sigma-h_M & \text{if side } M \text{ is type 3.}\end{cases}$$

A boundary of type 0 designates a far-away boundary, as in a semi-infinite body. The derivation of the Fourier-space GF in Eq. (6) parallels that for steady-state GF given elsewhere [20]; however, in the present work σ is complex.

This form of the GF is particularly well-behaved for machine computation, and most importantly, the temperature expressions based on these GF are similarly well-behaved for any layer thickness and for any frequency. This is a key contribution of this paper, in sharp contrast with previously reported difficulties in evaluating numerical values from exact solutions. For example, numerical overflow can occur with other formulations in thermally thick layers [13]. In a time-domain study, only short-time results were included due to numerical difficulties associated with longer times [3].

The GF expression given in Eq. (6) covers a number of boundary condition combinations, and a numbering system is used to distinguish among them. Designation XIJ is used to identify the GF for heat transfer in a layer with boundary condition of type I = 1, 2, or 3 at $x=0$ and

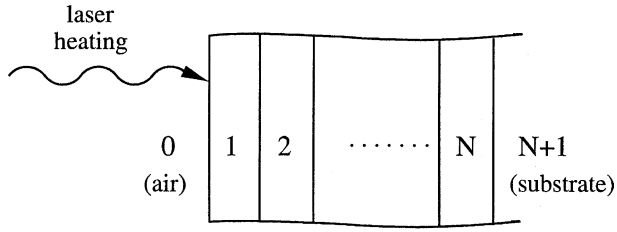

Fig. 1. Multilayer geometry heated by laser absorption.

with boundary condition of type $J = 1$, 2, or 3 at $x = L$. For example, designation X12 represents the GF with type 1 boundary at $x = 0$ and type 2 boundary at $x = L$. Designation XI0 is used to identify the GF for a semi-infinite region. For example, designation X20 represents the GF for a semi-infinite body with a boundary of type 2 at $x = 0$.

4. TEMPERATURE IN LAYERED MATERIALS

In this section the temperature caused by absorption of laser energy will be found in a domain consisting of non-absorbing air, N solid layers, and a substrate. The geometry is shown in Fig. 1. At the interfaces, let q_{nm} represent the heat flux leaving layer n and entering layer m. Applying Eq. (5), the interface temperature in the air is

$$T_0(0, \omega) = \frac{\alpha_0}{k_0} G_0(0, 0, \omega) q_{10}. \tag{7}$$

In layer i, $i = 1, 2, \ldots, N$: the interface temperatures are

$$T_i(0, \omega) = \frac{\alpha_i}{k_i} G_i(0, 0, \omega) q_{i-1,i} + \frac{\alpha_i}{k_i} G_i(0, L_i, \omega) q_{i+1,i} + B_i(0), \tag{8}$$

$$T_i(L_i, \omega) = \frac{\alpha_i}{k_i} G_i(L_i, 0, \omega) q_{i-1,i} + \frac{\alpha_i}{k_i} G_i(L_i, L_i, \omega) q_{i+1,i} + B_i(L_i). \tag{9}$$

In the substrate the temperature at the interface is

$$T_{N+1}(0, \omega) = \frac{\alpha_{N+1}}{k_{N+1}} G_{N+1}(0, 0, \omega) q_{N,N+1} + B_{N+1}(0). \tag{10}$$

In the above expressions, symbol B_i has been used for the volume-heating integral term from Eq. (5), specifically,

$$B_i(x) = \frac{\alpha_i}{k_i} \int_{x'} g(x', \omega) G_i(x, x', \omega)\, dx'. \tag{11}$$

Here g is the laser energy absorbed in the layer per unit volume; this can be determined without approximation from an optical calculation taking into account the absorption in each layer, the transmission through each layer interface, and the multiple internal relections from each layer interface [11]. For the two examples discussed later in this paper, the surface layer is opaque and the optical absorption takes place entirely at the surface. In these cases the volumetric heating in the first layer is given by $g = q_L \cdot \delta(0)$ where q_L is the (Fourier-space) flux of laser energy entering the sample ($\mathrm{W \cdot s \cdot m^{-2}}$) and δ is the Dirac delta function.

In the above temperature expressions, all of the interface heat fluxes are initially unknown. The heat flux leaving one layer enters the adjacent layer, $q_{i-1,i} = -q_{i,i-1}$, and the temperature difference between adjacent layers is related to heat flux through a contact resistance at each interface:

$$q_{i-1,i}\, R_i = T_i(0,\omega) - T_{i-1}(L_{i-1},\omega), \quad i = 1, 2, \ldots, N+1. \tag{12}$$

The contact resistance R_i describes the size of the temperature jump across the interface. Next Eqs. (7)–(10) are combined with Eq. (12) to eliminate temperature. The result is a set of $N+1$ linear algebraic equations for the unknown heat fluxes, which may be stated in matrix form:

$$\begin{bmatrix} W_0+U_1+R_1 & -V_1 & 0 & \ldots & 0 \\ -V_1 & U_1+U_2+R_2 & -V_2 & \ldots & 0 \\ 0 & -V_2 & U_2+U_3+R_3 & \ldots & 0 \\ \ldots & \ldots & \ldots & \ddots & -V_N \\ 0 & 0 & \ldots & -V_N & U_N+W_{N+1}+R_{N+1} \end{bmatrix} \times \begin{bmatrix} q_{10} \\ q_{21} \\ q_{32} \\ \cdots \\ q_{N+1,N} \end{bmatrix} = \begin{bmatrix} B_1(0) \\ B_2(0)-B_1(L_1) \\ B_3(0)-B_2(L_2) \\ \cdots \\ B_{N+1}(0)-B_N(L_N) \end{bmatrix}. \tag{13}$$

Symbols W_i, U_i, and V_i used in the above expression are given below:

$$\begin{aligned} W_i &= \frac{\alpha_i}{k_i} G_i(0,0,\omega), \\ U_i &= \frac{\alpha_i}{k_i} G_i(0,0,\omega) = \frac{\alpha_i}{k_i} G_i(L_i, L_i, \omega), \\ V_i &= \frac{\alpha_i}{k_i} G_i(0, L_i, \omega) = \frac{\alpha_i}{k_i} G_i(L_i, 0, \omega). \end{aligned} \tag{14}$$

For any multi-layered system, it is now possible to calculate the heat fluxes (q_{ij}) through all interfaces in the system. The above result is *exact*, and

Cramer's rule may be used to solve for the q–values for a sample composed of one or two layers. For a sample with two or more layers, a numerical matrix solution is best. Once the heat fluxes are found, the temperature at any interface is given by Eqs. (8)–(10), or the temperature within any layer may be found with Eq. (5).

Several different GF may be used in the above matrix equation. The non-absorbing gas (region 0) is a semi-infinite region so the GF needed is number X20. For layers $i=1, 2, \ldots, N$, the GF needed is type X22 (specified heat flux). The GF for the substrate depends on the heat transfer environment there. For example, a thick substrate could be described by GF number X20, or, a substrate in imperfect contact with a cold plate could be described by GF number X23.

5. OPTIMAL EXPERIMENT DESIGN

For the photothermal experiments discussed here, one or more temperatures, T_j, are to be measured directly, and several thermal properties, b_k, are to be deduced from these measurements. A good experiment is one with observed quantities (T_j) that are sensitive to the properties of interest (b_k). To optimize the experiment, it is important to quantify this sensitivity and seek the best sensitivity across a variety of (simulated) experimental conditions.

Consider a simulated experiment which contains several temperature sensors, and let quantity T_j be the output from the jth sensor. The experiment is repeated at several frequencies and data is available from all the sensors at each frequency. Let the sensitivity coefficients be defined by

$$X_{jk}(i) = b_k \frac{\partial T_j}{\partial b_k}, \tag{15}$$

which is the sensitivity for the kth parameter, the jth temperature sensor, and the ith frequency. Parameters b_k may include thermal conductivity, specific heat, density, etc. In this research the sensitivity coefficients have been computed from the real-valued amplitude and real-valued phase of the complex temperature at r frequencies, for which the distinct amplitude and phase values are treated as $2r$ measurements from each sensor.

The sensitivity coefficients were computed with a finite-difference procedure to approximate the derivative, as follows:

$$X_{jk}(i) \approx b_k \frac{[T_{ij}((1+\epsilon)b_k) - T_{ij}(b_k)]}{\epsilon b_k}. \tag{16}$$

Here T_{ij} is the temperature at the ith frequency for the jth sensor. The value of $\epsilon = 0.001$ was found to give well-behaved values for X.

In a good experiment, there are two specific requirements that the sensitivity coefficients must satisfy. First, the sensitivity coefficients should be as large as possible. Second, when two or more parameters are to be measured in the same experiment, the sensitivity coefficients must be linearly independent. A formal procedure to quantify these two requirements may be constructed if the sensitivity coefficients are assembled into a sensitivity matrix $\boldsymbol{X}$, which is then multiplied by its transpose, given formally by $\boldsymbol{X}^T\boldsymbol{X}$, of size $[p \times p]$. The optimality criterion is the (normalized) determinant of matrix $\boldsymbol{X}^T\boldsymbol{X}$, given by [15]

$$D = \frac{1}{s\,r\,(T_{\max})^2} \det(\boldsymbol{X}^T\boldsymbol{X}). \tag{17}$$

Note that the optimality criterion D is normalized by the maximum temperature rise (squared), the number of sensors s, and the number of frequencies r. This is important so that D may be used to compare different experiments. When D is large, the sensitivity coefficients will be large and linearly independent [16].

6. RESULTS FOR A LAYERED MATERIAL

In this section the techniques of simulation and optimal experiment design are applied to a SiO_2 film on a Si substrate. An opaque coating of Ni of 20 nm thickness was added to the sample so that all optical absorption would take place at the sample surface. This material has been studied elsewhere by a photoacoustic acoustic technique over a frequency range from 2000 to 20,000 Hz, and the measured thermal conductivity of the SiO_2 film and the contact resistance between the film and the Si substrate are: $k = 1.52$ W·m^{-1}·K^{-1} and R $< 10^{-9}$ K·m^2·W^{-1} [13].

Using the present methods, the computed phase of the surface temperature agrees very well with published values, as shown in Fig. 2, thus verifying the present approach. The property values used for the computation are given in Table I. Note that the actual experimental values published in Ref. 13 are the phase of the acoustic response of the Ni/SiO_2/Si sample, and these values have been shifted by 45 ° to give the experimental values for the phase of the surface temperature shown in Fig. 2. Amplitude values are not shown because the property values taken from Ref. 13 were determined from phase measurements only.

The sensitivity coefficients for the phase of the surface temperature to variations in the conductivity of the SiO_2 layer, k, and the contact resistance with the Si substrate, R, are plotted in Fig. 3. The sensitivity to conductivity k has a maximum (negative) value at about 6000 Hz. The shape of the R-sensitivity curves and the location of the largest value

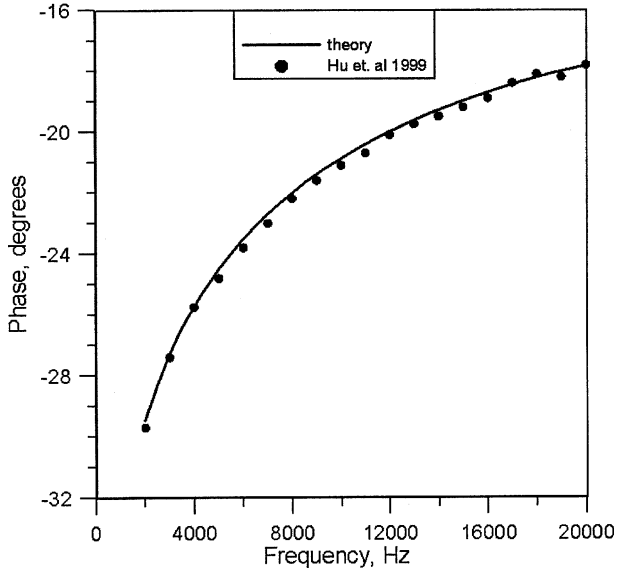

Fig. 2. Comparison between present theory and experimental values of Ref. 13 for the phase of surface temperature for a $Ni/SiO_2/Si$ sample.

Table I. Properties Used in Calculations of a Three-layer Solid which is Heated at the Ni Surface and Exposed to a Layer of Air on Either Side

Layer	i	d (μm)	k ($W \cdot m^{-1} \cdot K^{-1}$)	α ($m^2 \cdot s^{-1}$)	R ($K \cdot m^2 \cdot W^{-1}$)
Air	0	–	0.0263	2.25E-05	–
Ni	1	0.07	80	1.98E-05	0
SiO_2	2	0.485	1.52	9.09E-07	0
Si	3	382	151	9.09E-04	Varies
Air	4	–	0.0263	2.25E-05	–

depends strongly on the R value. For $R = 10^{-8}$–10^{-7}, the sensitivity curves are relatively small, with a broad peak near 3000 Hz. For $R = 10^{-6}$, however, the sensitivity values are large and positive at small frequencies and the curve slopes down to negative values as frequency increases. Some conclusions for $R < 10^{-7}$ are that the sensitivity coefficient is small, but the frequency range considered (500–20,000 Hz) captures the peak sensitivity. For $R = 10^{-6}$ the largest sensitivity may lie outside this frequency range.

Next the sensitivities for k and R will be examined together. Optimality criterion D provides a numerical measure of the extent to which

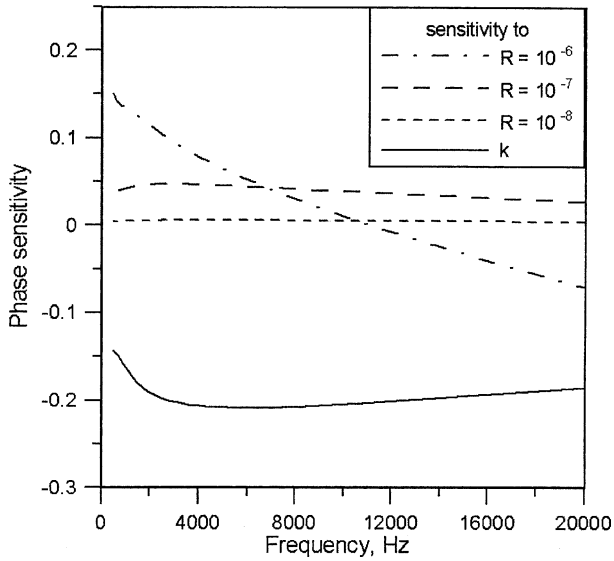

Fig. 3. Phase sensitivity to thermal conductivity and to layer-substrate contact resistance for a layer of SiO_2 on silicon at various frequencies.

the sensitivity coefficients are both large and linearly independent, and at which frequencies this occurs. Figure 4 shows the optimality criterion for the layered material for both thermal conductivity and contact resistance considered together. The highest curve is for k and $R = 10^{-6}$, and the peak for this curve is about 4000 Hz. For the $R = 10^{-7}$–10^{-8} curves the peak occurs around 8000 Hz. Figure 4 indicates that the best experiment to measure both k and R when $R = 10^{-6}$ includes data at 4000 Hz. For smaller R-values the most important frequency is 8000 Hz, however, because D is smaller the analysis of the data may be more difficult. It is important to note that each point on Fig. 4 represents a value for D computed from a range of data extending from 20,000 Hz down to that point; data is added from high frequency to low frequency. To repeat, the D-values indicate what frequency range is needed for optimal estimation of both k and R from experimental data.

7. RESULTS FOR A FUNCTIONALLY GRADED MATERIAL

In this section the methods for experimental design are applied to a two-phase ceramic/ceramic material with graded volume fractions of the

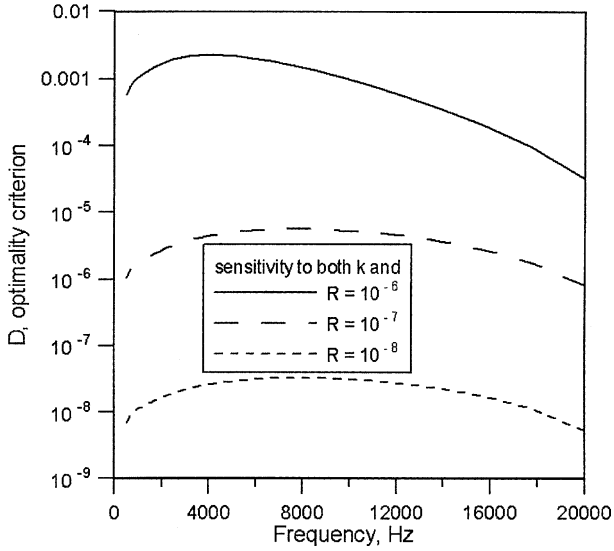

Fig. 4. Optimality criterion D for simultaneous estimation of thermal conductivity and contact resistance, versus frequency, for a layer of SiO_2 on silicon.

components. The volume fraction profile is assumed to have the form,

$$V_1(x) = 1 - (x/L)^p, \qquad V_2(x) = (x/L)^p, \tag{18}$$

where V_1 and V_2 are the volume fractions of the components. At $x = 0$ the material is pure component 1 and at $x = L$ the material is pure component 2. The particular material considered is composed of TiC and SiC, and the thermal properties are given in Table II. The thermal conductivity of the material is given by

$$k(x) = k_1 \left[1 + \frac{V_2(x)(k_2 - k_1)}{k_1 + (k_2 - k_1)V_1(x)/3} \right], \tag{19}$$

where subscripts 1 and 2 stand for the properties of components 1 and 2, respectively. Figure 5 shows the spatial distribution of conductivity for the TiC/SiC material for several values of exponent p. The mass density and specific heat are determined by the rule of mixtures:

$$\rho(x) = V_1(x)\rho_1 + V_2(x)\rho_2, \tag{20}$$

$$c(x) = V_1(x)c_1 + V_2(x)c_2. \tag{21}$$

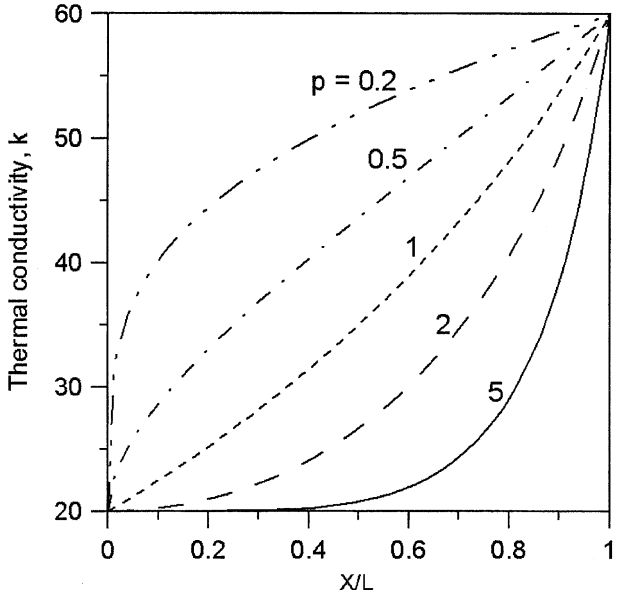

Fig. 5. Thermal conductivity distribution in a functionally graded material for several values of distribution parameter p.

Table II. Material Properties of TiC and SiC

	Material	k $(W \cdot m^{-1} \cdot K^{-1})$	ρ $(kg \cdot m^{-3})$	c $(J \cdot kg^{-1} \cdot K^{-1})$
1	TiC	20	4900	700
2	SiC	60	3200	1000

The thermal-stress behavior of this material has previously been studied [3].

In photothermal methods, the sample is heated by a periodically modulated laser beam, and the surface temperature (or a subsequent acoustic signal) is measured at the modulation frequency. The temperatures reported below are computed with the layered GF method with 50 layers used to simulate the spatial variation in the sample. Both surfaces of the sample are exposed to air. The surface temperature is shown in Fig. 6a (amplitude) and b (phase) versus dimensionless frequency. The frequency is normalized as $f^* = fL^2/\alpha_{av}$ where L is the material thickness and $\alpha_{av} = (\alpha_1 + \alpha_2)/2$, the average of the component values. In Fig. 6 the sample is heated at $x = 0$ and the temperature is reported at $x = 0$, the low-k side.

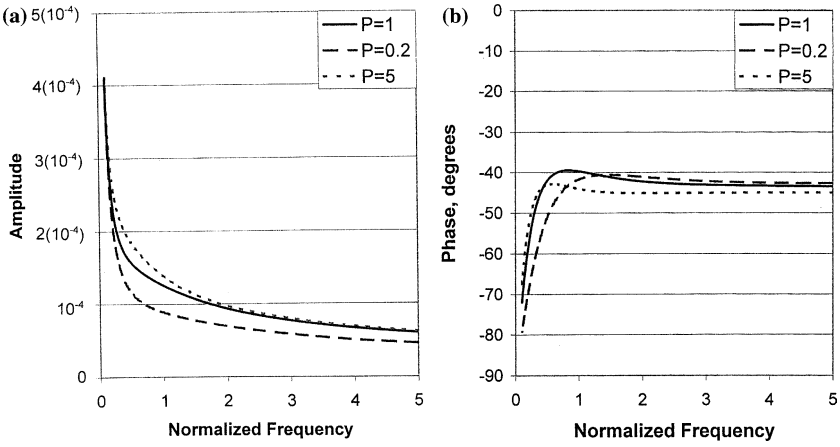

Fig. 6. Surface temperature (a) amplitude and (b) phase versus dimensionless frequency for a functionally graded material heated periodically at the surface.

This heating condition provides slightly higher temperature response than for heating on the high-k side (at $x = L$). Note that in Fig. 6a the amplitude curves are monotonic with few distinguishing features. In contrast the phase has a distinctive maximum for each p value, which supports the experimental observation that phase is more important than amplitude for photothermal measurement of thermal properties.

Figure 7a shows the sensitivity of the phase of temperature to k_2, the thermal conductivity of component 2, for three values of the spatial distribution parameter p. Note that the sensitivity is largest for $p = 1$, the linear k-distribution, and is small for other distributions. In Fig. 7a the peak sensitivities are located in a range of dimensionless frequencies below $f^* = 1$. This range of frequencies represents thermal waves (generated by the periodic heating) that penetrate all the way through the sample thickness. The sensitivity to k_1, the component 1 thermal conductivity, is not shown because it is similar in size and shape to the k_2 sensitivities (but values are negative).

Figure 7b shows the sensitivity of the phase of the temperature to the spatial distribution parameter p. The curve for $p = 1$ has a large positive peak at about $f^* = 0.2$ and a negative peak at about $f^* = 1.5$. The largest sensitivities are again located in the range $f^* < 1$. The normalized sensitivity of the *amplitude* of the temperature, not shown, is two orders of magnitude smaller than the normalized sensitivity for the phase, again indicating that phase is more important than amplitude for experimental thermal property determination.

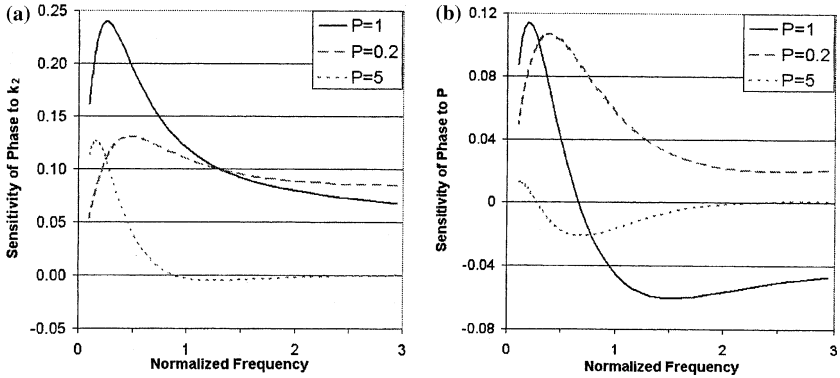

Fig. 7. Sensitivity of the phase of temperature to (a) conductivity k_2 and (b) exponent p for the functionally graded material heated periodically at the surface.

The sensitivity to a single parameter is useful for determining a single parameter from an experiment. When two or more parameters are to be determined, optimality criterion D is instructive. Figure 8a shows optimality criterion D for both conductivity k_2 and exponent p. Both amplitude and phase information was used to compute these values. The largest curve is for $p=1$ which indicates that this spatial distribution will provide better estimates of thermal properties k_2 and p from an experiment than for other p-values. The location of the peak for each curve indicates which frequencies should be included in an experiment. Since the D-values shown were computed from high-to-low frequencies, the peak indicates the lowest frequency of data that is needed for optimal data analysis.

Optimality criterion D was also investigated for other combinations of parameters. The D-values computed for p and k_1 together, not shown, were identical to Fig. 6a, which is expected from the similarity in the shape of the sensitivities to k_1 and k_2 mentioned earlier. The D-values computed for k_1 and k_2 together are shown in Fig. 8b. The important feature of this figure is the vanishingly small values, five orders of magnitude smaller than Fig. 8a values, which indicates that k_1 and k_2 should not be sought simultaneously. As mentioned before the sensitivity coefficients for k_1 and k_2 have a similar shape, so the fact that their combined D-value is near zero reinforces the idea that the sensitivities for k_1 and k_2 are not linearly independent. Finally, D-values were also computed for p, k_1, and k_2 considered simultaneously (not shown), and these values were predictably near zero because of the dependence of k_1 and k_2.

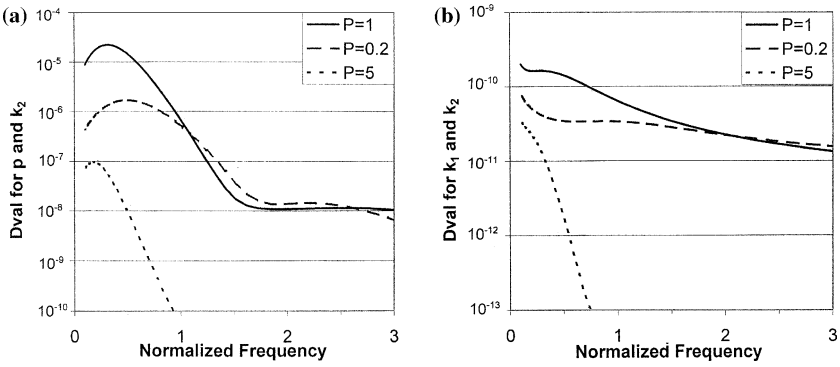

Fig. 8. Optimality criterion D for simultaneous estimation of (a) conductivity k_2 and distribution parameter p, and (b) conductivities k_1 and k_2, for the functionally graded material.

8. SUMMARY

This paper investigates photothermal methods for thermal characterization of functionally graded materials through numerical modeling and experiment design. No laboratory experiments are reported here. A new formulation is given for the temperature response of layered materials to periodic heating, based on the method of Green's functions, which is numerically better behaved than previous work. The method has been applied to a SiO_2 layer on silicon and compared to literature values to validate the method. Optimality criterion D indicates which frequency range of experimental data should provide the best possible estimates of the layer conductivity and contact conductance.

The new methods have also been applied to a two-component functionally-graded material with a power-law distribution of thermal properties. The largest temperature response is found by heating the sample on the low-k side, and the phase of the temperature is particularly important for estimation of thermal properties. Component conductivities k_1 and k_2 have similar-shaped sensitivity coefficients, and consequently both cannot be estimated simultaneously from experimental data. The most important parameter is p which describes the spatial distribution of thermal properties in the functionally-graded material. Values for optimality criterion D indicate that values for p may be found simultaneously with one of the conductivities, but not both. Dimensionless frequencies in the range $f^* < 1$ are important for measurement of spatial-distribution parameter p. The magnitude of the optimality criterion D also suggests that it will be easier to estimate parameters for $p \approx 1$ (near-linear spatial variation) compared to other values of p.

ACKNOWLEDGMENTS

This work was supported by NASA Langley grant NAG-1-01087 under the supervision of Max Blosser. The author would like extend thanks to Xinwei Wang for helpful discussions of photoacoustic methods and to Ryan Sneed for carrying out many numerical simulations. Mr. Sneed's salary was provided by the Undergraduate Creative Activity and Research Experiences (UCARE) program at the University of Nebraska.

NOMENCLATURE

B: integral term, Eq. (11)
c: specific heat ($J \cdot kg^{-1} \cdot K^{-1}$)
D: optimality criterion, Eq. (17)
f: known effect at boundary i
g: internal heating by optical absorption ($J \cdot m^{-3}$)
G: steady-periodic Green's function ($s \cdot m^{-1}$)
h: heat transfer coefficient, ($W \cdot m^{-2} \cdot K^{-1}$)
j: imaginary number, $\sqrt{-1}$
k: thermal conductivity ($W \cdot m^{-1} \cdot K^{-1}$)
L_j: thickness of layer i (m)
n: outward-facing unit normal vector on a boundary
p: number of parameters in simulated experiment
q: steady-periodic heat flux ($W \cdot s \cdot m^{-2}$)
r: number of frequencies in simulated experiment
R_i: contact resistance at interface i, ($K \cdot m^2 \cdot W^{-1}$)
s: number of sensors in simulated experiment
t: time (s)
T: steady-periodic temperature ($K \cdot s$)
U, V, W: boundary-evaluated Green's functions, Eq. (16)

Greek

α: thermal diffusivity ($m^2 \cdot s^{-1}$)
δ: Dirac delta function (m^{-1})
ρ: density ($kg \cdot m^{-3}$)
σ: $\sqrt{j\omega/\alpha}$
ω: frequency ($rad \cdot s^{-1}$)

Superscripts

$\tilde{(\,)}$: time-domain quantity

Subscripts

0: gas region above sample
i: index for layer or for boundary

REFERENCES

1. T. Ishiguro, A. Makino, N. Araki, and N. Noda, *Int. J. Thermophys.* **14**:101 (1993).
2. K. S. Kim and N. Noda, *J. Therm. Stresses* **24**:457 (2001).
3. Z. H. Jin and G. H. Paulino, *Int. J. Fracture* **107**:73 (2001).
4. A. Sutradhar, G. H. Paulino, and L. J. Gray, *Eng. Anal. Boundary Elem.* **26**:110 (2002).
5. K. S. Kim and N. Noda, *JSME Int. J. Ser. A* **44**:31 (2001).
6. M. Ferrari, F. Rooney, and J. C. Nadeau, *Mat. Sci. Forum* **308–311**:989 (1999).
7. Y. Obata and N. Noda, *Arch. Appl. Mech.* **66**:581 (1996).
8. A. Makino and N. Noda, *Int. J. Thermophys.* **15**:729 (1994).
9. A. Makino and N. Noda, *Mat. Sci. Forum* **308–311**:896 (1999).
10. A. Mandelis, *Diffusion-Wave Fields, Mathematical Methods and Green's Functions* (Springer, New York, 2001).
11. W. A. McGahan and K. D. Cole, *J. Appl. Phys.* **72**:1362 (1992).
12. K. D. Cole and W. A. McGahan, *J. Heat Trans.* **155**:767 (1993).
13. H. Hu, X. Wang, and X. Xu, *J. Appl. Phys.* **86**:3953 (1999).
14. J. V. Beck and K. J. Arnold, *Parameter Estimation* (Wiley, New York, 1977).
15. R. Taktak, J. V. Beck, and E. P. Scott, *Int. J. Heat Mass Trans.* **36**:2977 (1993).
16. K. J. Dowding and B. F. Blackwell, *J. Heat Trans.* **123**:1 (2001).
17. K. D. Cole, *J. Thermophys. Heat Trans.* **18**:289 (2004).
18. A. Mandelis, *J. Appl. Phys.* **78**:647 (1995).
19. J. V. Beck, K. D. Cole, A. Haji-Sheikh, and B. Litkouhi, *Heat Conduction Using Green's Functions* (Hemisphere, New York, 1992).
20. P. E. Crittenden and K. D. Cole, *Int. J. Heat Mass Trans.* **45**:3583 (2002).